LAWRENCE
LIVERMORE
NATIONAL
LABORATORY

UCRL-PROC-231695

Effect of High Temperature Aging on the Corrosion Resistance of Iron Based Amorphous Alloys

S. D. Day, J. J. Haslam, J. C. Farmer, Raul B. Rebak

June 12, 2007

Materials Science and Technology 2007 Conference and Exhibition
Detroit, MI, United States
September 16, 2007 through September 20, 2007

Effect of High Temperature Aging on the Corrosion Resistance Of Iron Based Amorphous Alloys

S. D. Day, J. J. Haslam, J. C. Farmer and R. B. Rebak
Lawrence Livermore National Laboratory
Livermore, California, USA

Keywords: Iron Amorphous Alloys, Thermal Stability, Seawater, Corrosion, 316SS, C-22

Abstract

Iron-based amorphous alloys are more resistant to corrosion than polycrystalline materials of similar compositions. However, when the amorphous alloys are exposed to high temperatures they may recrystallize (or devitrify) thus losing their inherent resistance to corrosion. Four different types of amorphous alloys melt spun ribbon specimens were exposed to several temperatures for short periods of time. The resulting corrosion resistance was evaluated in seawater at 90°C and compared with the as-prepared ribbons. Results show that the amorphous alloys can be exposed to 600°C for 1-hr. without losing the corrosion resistance; however, when the ribbons were exposed at 800°C for 1-hr. their localized corrosion resistance decreased significantly.

Introduction

Metallic amorphous alloys or metallic glasses have been studied extensively for the last three decades due to their unique characteristics, including superior mechanical properties and corrosion resistance [1]. To produce an amorphous alloy from a liquid state, cooling rates in the order of 10^6 to 1 degrees Kelvin per second are required, depending on the glass forming ability of the melt [1]. The amorphous alloys are chemically and structurally homogeneous since they do not contain grain boundaries, dislocations and secondary phases, which are common in the crystalline materials [1]. The corrosion resistance of amorphous alloys depends on the alloy composition [2-4]. Amorphous alloys are more corrosion resistant than their polycrystalline cousins of equivalent composition. Amorphous alloys are hard and can be used in areas where both resistance to wear and corrosion are simultaneously needed. For example the typical Vickers hardness of the polycrystalline Alloy 22 (N06022) is 250 but the Vickers hardness of an amorphous material is higher than 1000 [5]. The fact that amorphous materials are highly corrosion resistant is generally attributed to the absence of crystalline defects in the alloy; however the actual mechanism of this resistance is still not fully understood [1]. When amorphous alloys partially or fully re-crystallize, they may lose some of their characteristic corrosion resistance. This process is called devitrification [6].

Iron (Fe) based alloys such as austenitic stainless steels containing approximately 18% chromium (Cr) are widely used in the industry due to their corrosion resistance characteristics.

However, polycrystalline Types 304 and 316 stainless steels are not as corrosion resistant as other polycrystalline alloys such as the nickel (Ni)-based Hastelloy C-22 alloy (Table 1) [7]. On the other hand, Fe-based amorphous alloys have even higher localized corrosion resistance than Alloy C-22 [8]. Since the iron based amorphous alloys are more economical to produce than the highly corrosion resistant nickel based alloys, its use seems attractive just for economical reasons.

Recently, Fe-based amorphous alloys have been produced in bulk compositions so they can be applied to the fabrication of many large structural components, including oceanic shipbuilding, nuclear, and oil and gas industries. These alloys are called structural amorphous metals or SAM by DARPA (Defense Advanced Research Projects Agency). Fe is a desirable base element for alloys that may be used in large industrial applications not only because Fe is inexpensive but also because Fe-based bulk metallic glasses have a high glass forming ability, high mechanical properties and soft magnetic properties. [9] The newer Fe-based amorphous alloys can be produced at relatively slow cooling rates on the order of 100 Kelvin per second [10]. This allows the production of bulk amorphous metals tailored to specific applications using processes such as thermal spray. Fe-based amorphous alloys such as SAM2X5 may contain up to 15% (atomic) in boron (B), which make them attractive for nuclear applications as neutron absorbing structural material [11]. SAM2X5 is a candidate material for neutron absorption applications and a candidate to replace both borated stainless steels and recently developed nickel-chromium-molybdenum-gadolinium (Ni-Cr-Mo-Gd) alloys. Another Fe-based amorphous (SAM1651) alloy contains more molybdenum (Mo) for enhanced corrosion resistance [12]. It has been recently shown that, when the amorphous alloys are forced to corrode by polarization, their dissolution pattern is uniform while the polycrystalline materials such as Alloy 22 dissolve in a non-uniform manner following grain boundaries and other microstructural discontinuities pertaining wrought alloys [13].

The aim of the current study was to evaluate the thermal stability of the amorphous alloys ribbons. Devitrification was assessed using electrochemical tests in seawater at 90°C.

Experimental

Table 1 shows the nominal chemical composition of the studied alloys. There were two polycrystalline engineering alloys (316SS or S31600 and Alloy 22 or N06022) and four amorphous alloys. The polycrystalline specimens were cut from thick wrought plates in disc form (as described in ASTM G 5) [14] and in multiple crevice assembly (MCA) form. The amorphous alloys were small ribbons approximately 20 to 50 mm long, 1 mm wide and 25 μm thick (Figure 1). The test area of the ribbons was approximately 0.4 to 1 cm^2. The ribbons were prepared by dropping molten metal on a water-cooled copper spinning wheel in an inert atmosphere. The initial metal temperature was 1050°C and the wheel was spinning at 17.5 m/sec. The fast cooling fabrication process made the material amorphous. The ribbon had two sides; the side that contacted the spinning wheel was slightly darker and contained small dent-like features and the side that faced away from the wheel was smoother and highly reflective (shiny).

Ribbons were thermally aged in controlled atmosphere mostly at 600°C, 800°C and 1000°C. The thermal aging time was generally 1 hour. A few tests were conducted for 5 minutes at 600°C and others for 5 hours at 150°C.

Table 1. Chemical Composition of the Studied Alloys.

Alloy	Approximate Composition A – Weight %, B – Atomic %	Type of Alloy, Specimen
316 SS	70Fe-18Cr-10Ni-2.5Mo [A]	Polycrystalline, Disc
C-22	57Ni-22Cr-13Mo-3W-3Fe [A]	Polycrystalline, Disc and MCA
DAR40	52.3Fe-19Cr-16B-4C-2.5Si-2.5Mo-2Mn-1.7W [B]	Amorphous, Melt Spun Ribbon
SAM2X3	50.7Fe-18.4Cr-15.5 B-5.4Mo-3.9C-2.4Si-1.9Mn-1.6W [B]	Amorphous, Melt Spun Ribbon
SAM2X5	49.7Fe-18.1Cr-15.2 B-7.4Mo-3.8C-2.4Si-1.9Mn-1.6W [B]	Amorphous, Melt Spun Ribbon
SAM1651	48Fe-15Cr-14Mo-6B-15C-2Y [B]	Amorphous, Melt Spun Ribbon

A three-electrode cell (Figure 1), with a capacity of one liter, was used for all the experiments. Generally, 900 mL of electrolyte solution was used in each test. A saturated silver/silver chloride (Ag/AgCl, pre-filled with 4 M KCl saturated with AgCl) reference electrode was used for measuring the potential of the working electrode. The tests were conducted in natural seawater removed from the Pacific Ocean off the shore of Half Moon Bay (just south of San Francisco). Tests were conducted in seawater heated to 90°C. The bridge between the reference electrode and the Luggin capillary was also filled with seawater. A water cooled jacket was used to maintain the reference electrode at near room temperature. A platinum (Pt) sheet welded to a Pt wire was used as a counter electrode. The electrochemical cell was heated using a heating mantle. Nitrogen gas was bubbled through the test solution for deaeration. The gas exited the cell though a condenser and a liquid trap to prevent evaporation of the solution and the ingress of air into the test cell. The deaeration was started 24 hour before the electrochemical tests. During this period the evolution of the corrosion potential was monitored. The electrochemical polarization measurements were conducted through a commercial potentiostat that was integrated with a desktop computer and the companion software.

The electrochemical test sequence consisted of three steps; (1) Monitoring the corrosion potential for 24 h, (2) Three consecutive polarization resistance tests (ASTM G 59 and G 102) [14], and (3) A cyclic potentiodynamic polarization (CPP) (ASTM G 61) [14] test. For the polarization resistance and the CPP polarization tests, a potential scan rate of 600 mV per hour (0.167 mV/s) was used. In the polarization resistance tests the potential was scanned from 20 mV below the instantaneous corrosion potential to 20 mV above the corrosion potential. This test lasts approximately 4 minutes. For the CPP tests the scan was started at 100 mV below the instantaneous corrosion potential and the scan was reversed when the current density reached 5 mA/cm² or 1.2 V. From the CPP tests several parameters can be obtained. These parameters are grouped into (1) Breakdown potentials (E20 and E200, which are the potentials in the forward scan that need to be reached to obtain current densities of 20 and 200 μA/cm² respectively) and (2) Repassivation potentials (ER10, ER1 and ERCO). ER10 and ER1 are the potentials in the reverse scan that need to be reached to obtain current densities of 10 and 1 μA/cm². ERCO is the potential at which the reverse scan crosses over (CO) the forward scan.

The corrosion rate was estimated from the polarization resistance tests using the following formulas given in ASTM standards G 59 and G 102 [14]

$$i_{corr} = \frac{1}{R_p} \times \frac{b_a \cdot b_c}{2.303(b_a + b_c)}$$

$$CR(\mu m / yr) = k \frac{i_{corr}}{\rho} EW$$

where k is a constant (3.27 x 10^{-3} mm g/μA cm yr). The Tafel constants b_a and b_c were assumed to be ± 120 mV/decade, the density (ρ) of all the amorphous alloys were taken as 8 g/cm³ and the equivalent weight (EW) as 25.5-dimensionless.

Results

Corrosion Potential and Corrosion Rate of Ribbons

Figure 2 shows the evolution of the corrosion potential for two amorphous alloys (DAR40 and SAM2X5) in deaerated seawater at 90°C. For the as produced DAR40 and the 5 min.-aged at 600°C SAM2X5 ribbons the potential slightly increased as the immersion time increased. After 24-hr immersion the corrosion potential for these two specimens was on the order of -200 to -300 mV SSC. On the other hand the potential for the 1-hr aged at 800°C for both materials was on the order of -700 mV SSC. The values of corrosion potential suggest that the 1-hr aged at 800°C ribbons were more active than the as-produced DAR40 ribbon and the 5-min. aged at 600°C SAM2X5 ribbon. It is likely that the 1-hr aged at 800°C ribbons were devitrified and therefore were less resistant to corrosion. Table 2 shows the corrosion potential after 24-hr immersion. All the ribbon specimens aged at 800°C and 1000°C showed in general lower corrosion potential than the ribbons which were as-produced or aged at 600°C for 5 min. and at lower temperatures.

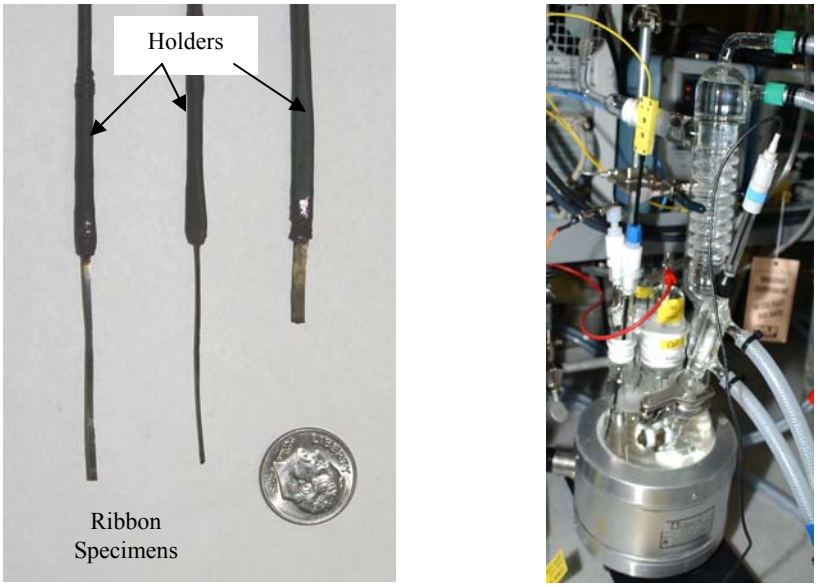

Figure 1. Ribbon Specimens and Testing Cell

Table 2. Experimental Results in Seawater at 90°C

Alloy	Aging Temp. (°C)	Aging Time (h)	E_{corr} 24-hr.	Average CR (μm/year)	E20 mV SSC	E200 mV SSC	ER10 mV SSC	ER1 mV SSC	ERCO mV SSC
DAR40	None	N/A	-295	0.235	983	1073	893	758	733
DAR40	None	N/A	-309	0.369	933	1055	878	766	773
DAR40	None	N/A	-100	0.516	930	1056	862	680	718
DAR40	150	5	-451	0.557	961	1058	869	722	748
DAR40	300	1	-346	0.258	928	1048	872	730	768
DAR40	600	0.083	-521	2.832	965	1060	879	733	862
DAR40	600	0.083	-542	3.395	945	1073	871	733	859
DAR40	600	1	-562	4.157	886	1091	838	571	849
DAR40	600	1	-370	0.909	897	1092	868	708	900
DAR40	800	1	-673	4.980	-361	-343	-536	-544	-544
DAR40	1000	1	-482	13.663	-189	-61	-425	-463	-467
DAR40	1000	1	-437	2.924	-296	-251			
SAM2X3	None	N/A	-214	0.310	962	1071	832	657	695
SAM2X3	600	0.083	-510	0.072					
SAM2X3	600	0.083	-362	1.564	923	1059	871	748	836
SAM2X3	600	1	-178	0.484	836	1105	877	751	914
SAM2X3	600	1	-291	0.084					
SAM2X3	600	1	-498	3.505	829	1063	868	726	924
SAM2X3	800	1	-674	1.426	263	267	-338	-361	-361
SAM2X3	1000	1	-590	0.168					
SAM2X5	None	N/A	-182	0.200	923	1200	913	845	957
SAM2X5	600	0.083	-182	0.244	974	1085	926	818	912
SAM2X5	600	0.083	-301	0.511	941	1036	906	781	903
SAM2X5	600	1	-503	0.053					
SAM2X5	600	1	-281	0.019	1175	1200	1110	909	1009
SAM2X5	600	1	-649	2.222	847	1044	941	851	1158
SAM2X5	800	1	-679	8.567	-375	-355	-539	-553	-553
SAM2X5	1000	1	-403	2.282	-295	-200			
SAM1651	None	N/A	-303	0.858	891	1015	649	448	550
SAM1651	600	0.083	-292	0.472	921	1025	666	389	642
SAM1651	600	0.083	-442	1.578	586	775	752	353	1115
SAM1651	600	1	-240	0.164	934	1026	728	520	686
SAM1651	600	1	-273	0.347	515	726	199	59	51
SAM1651	800	1	-526	3.511	317	381	-301	-348	-348
SAM1651	1000	1	-488	0.371	10	236	-278	-391	-404
316SS Disc	None	N/A	-223	0.014	144	146	-91	-204	
C-22 Disc	None	N/A	-318	3.031	414	673	440	-122	852
C-22 MCA	None	N/A	-478	4.472	371	509	-6	-68	-49

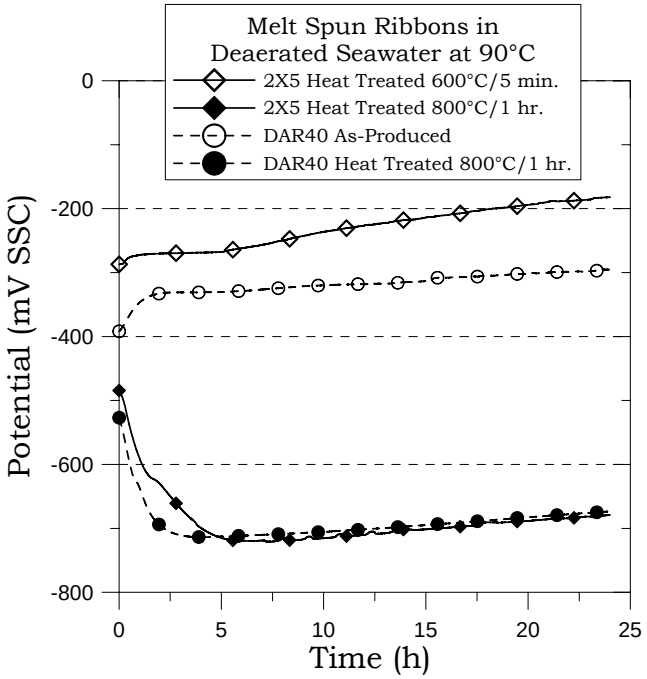

Figure 2. Corrosion potential as a function of immersion time

Table 2 also shows the average corrosion rate. As stated above, the corrosion rate was calculated using the polarization resistance test (ASTM G 59). Three consecutive tests were performed for each specimen in Table 2. The fitting of the data to calculate Rp was carried out using a ±10 mV potential range with respect to the instantaneous corrosion potential. The average value of the corrosion for three measurements is reported in Table 2. There is a large scattering in the values of the corrosion rates. These corrosion rates are for a short immersion time in deaerated seawater and they do not represent the long-term behavior of these alloys in the environment of testing. Nevertheless, some of the highest corrosion rates for the ribbon specimens were for the thermally aged at 600°C and higher temperatures.

Comparative Anodic Polarization between Amorphous and Polycrystalline Alloys

Figure 3 shows the cyclic potentiodynamic polarization of two amorphous ribbons and two polycrystalline materials in seawater at 90°C. It is evident that both DAR40 and SAM2X5 can be polarized to higher potentials than either 316SS and Alloy 22 before breakdown occurs. At an applied potential in the vicinity of 150 mV SSC, 316SS suffers breakdown of passivity via both pitting corrosion and crevice corrosion (E20 = 144 mV SSC, Table 2) (Figure 4). The current for the Alloy 22 specimen starts to increase at a potential higher than 400 mV SSC (E20 = 414 mV SSC, Table 2). The increase in current for the Alloy 22 disc was not via localized corrosion but due to massive transpassivity. On the other hand the value of E20 for the amorphous DAR40 and SAM 2X5 alloys were higher than 900 mV SSC. Figure 3 also shows that the current density in the passive region of potentials was more than one order of magnitude lower for the amorphous alloys than for the polycrystalline alloys (316SS and N06022). Figure 5 shows the repassivation potential ER1 from the cyclic potentiodynamic polarization (CPP)

(Table 2) for the four amorphous alloys and the two polycrystalline alloys. It is evident that ER1 for the amorphous materials is at least 500 mV higher than for the polycrystalline materials 316SS and Alloy 22. That is, in the tested hot seawater, the four amorphous alloys were superior to localized corrosion initiation and propagation than for even the N06022 Alloy. For the data in Table 2 and Figure 5, the Alloy 22 creviced specimen suffered extensive crevice corrosion while the amorphous specimens were free from localized corrosion. It is difficult to compare the relative localized corrosion resistant among the amorphous alloys since none of them actually suffered localized corrosion in the as-prepared condition. In general the higher the chromium and molybdenum content the higher the resistance to localized corrosion. SAM1651 has a higher amount of molybdenum content but at the same time lower chromium and higher carbon than the SAM2X3 and SAM2X5 alloys. The breakdown potential E20 seems to be a function of the amount of chromium in the alloy. The E20 was the highest for the highest chromium content (DAR40) and the lowest for the lowest chromium content (SAM1651) (Table 2).

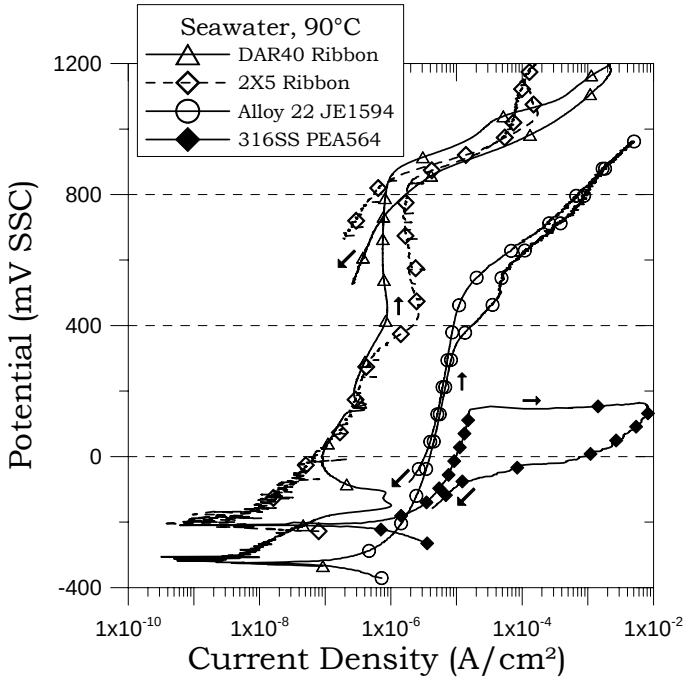

Figure 3. Cyclic potentiodynamic polarization(CPP) for amorphous and polycrystalline materials in seawater, 90°C

Figure 6 shows the cyclic potentiodynamic polarization for DAR40 material in three different conditions; (1) as-prepared, (2) thermally aged at 600°C for 1-hr and (3) thermally aged at 800°C for 1-hr. The highest corrosion potential and the lowest passive current density corresponded to the as-prepared material. Also, the breakdown potential E20 for the as-prepared ribbon was well above 800 mV SSC, suggesting a high resistance to passivity breakdown (Table 2). When the ribbons were aged at 600°C for 1-hr. the corrosion potential slightly decreased and the passive current density slightly increased (Figure 6). However, the breakdown potential E20 was still higher than 800 mV SSC (Figure 5 and Table 2) showing that a thermal treatment for 1-hr. at 600°C did not decrease the resistance of this alloy to localized corrosion. When the ribbon was aged for 1-hr. at 800°C the corrosion potential decreased even further and the passive current

density increased. Also, the breakdown potential E20 decreased dramatically to -361 mV SSC (Table 2 and Figure 5). It is apparent that this alloy suffered a loss in the corrosion resistance between a heat treatment at 600°C and at 800°C. It is likely that the alloy fully re-crystallized when it was exposed to 800°C for 1-hr. thus losing its corrosion resistance.

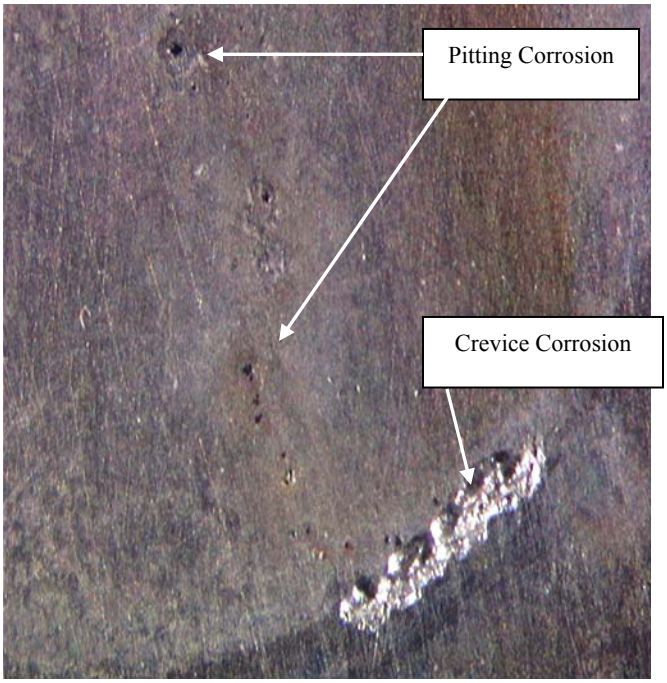

Figure 4. Pitting and crevice corrosion in 316SS disc in seawater at 90°C (specimen PEA564)

Effect of Thermal Aging on the Anodic Polarization of the Amorphous Alloys

Figure 7 shows the appearance of a non-treated ribbon after cyclic potentiodynamic polarization testing. The ribbon is free of corrosion products and any type of corrosion, general or localized even though this specimen was exposed to potentials higher than 1 V for long periods of time (Figure 6). The ribbon in Figure 6 appears dark but this is an optical effect. This ribbon was completely shiny and bright metallic but optical images are difficult to acquire on a shiny surface. Figure 8 shows the appearance of a 1-hr./800°C treated ribbon after the cyclic polarization test in seawater. This ribbon showed not only abundant rusting but also pitting corrosion. It is clear that the ribbon in Figure 8 appears more corroded than the ribbon in Figure 7 even though the former was only polarized to a maximum potential of less than -300 mV SSC (Table 2 and Figure 7). X-ray diffraction testing was not performed on the high temperature heat treated ribbon to confirm the transition from amorphous to crystalline, but the electrochemical data would indicate this transition.

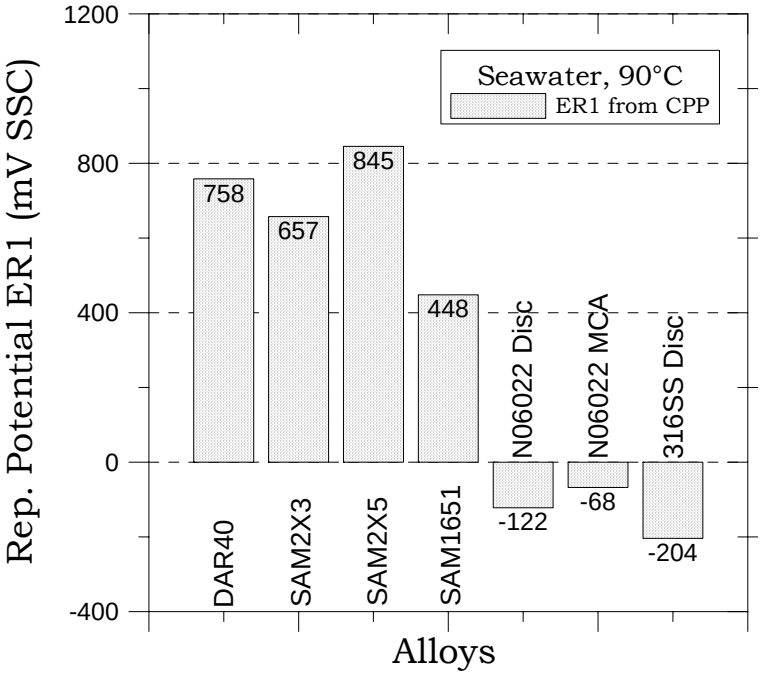

Figure 5. Repassivation potential ER1 for amorphous and polycrystalline materials

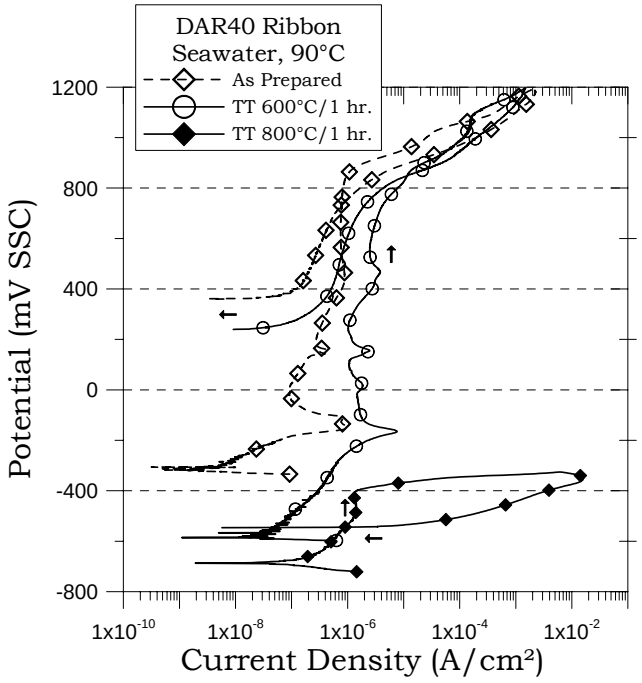

Figure 6. Cyclic potentiodynamic polarization for DAR40. Effect of thermal aging.

Figure 9 shows the repassivation potential ER1 for the four initially amorphous materials and the effect of heat treatment. Data is shown for (1) as-received ribbon, (2) aged at 600°C for 1-hr and (3) aged at 800°C for 1-hr. It is evident that there is not a loss of corrosion resistance

when the four materials were aged at 600°C for 1-hr. That it, for 1-hr. aging at 600°C the ER1 values were practically the same as for the as-prepared ribbon values (Figure 9 and Table 2). However, when the materials were aged at 800°C for 1-hr. there was a decrease in ER1 of approximately 800 mV (from +400 mV to -400 mV SSC). The values of ER1 for the thermally aged ribbons (Figure 8 and Table 2) are lower than the repassivation potential of the polycrystalline materials 316 SS and Alloy 22 (Table 2).

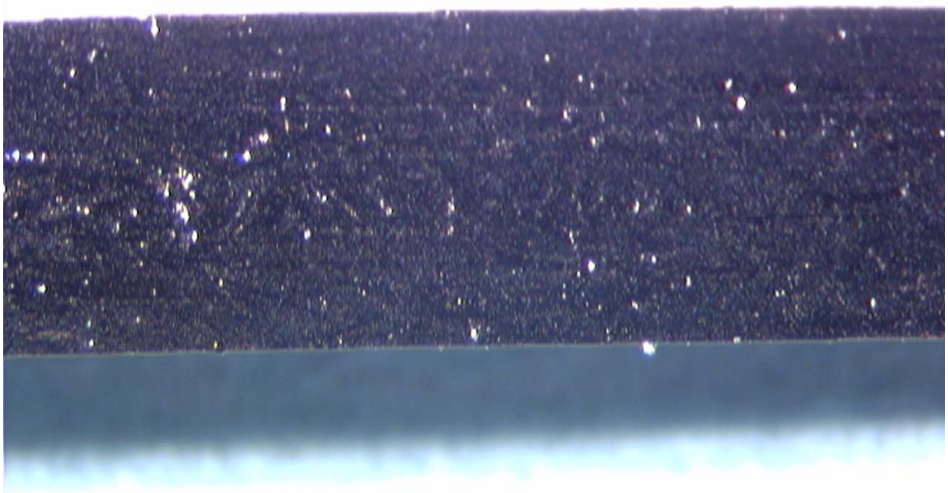

Figure 7. The as-prepared DAR40 ribbon after the cyclic potentiodynamic test. X20 Magnification

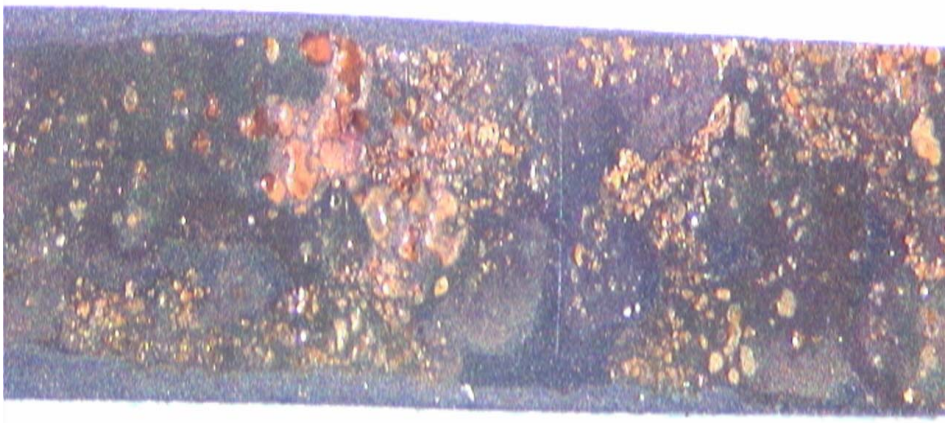

Figure 8. 1-hr./800°C aged DAR40 ribbon after the cyclic potentiodynamic test. X20 Magnification

Even though the four ribbon materials had slightly different chemical composition (Table 1), the data presented is not enough to make any judgment on the relative resistance to re-crystallization and the subsequent loss of corrosion resistance. More detailed studies of lower

temperatures and longer times may be needed to fully understand the mechanisms of re-crystallization and the effect on corrosion resistance.

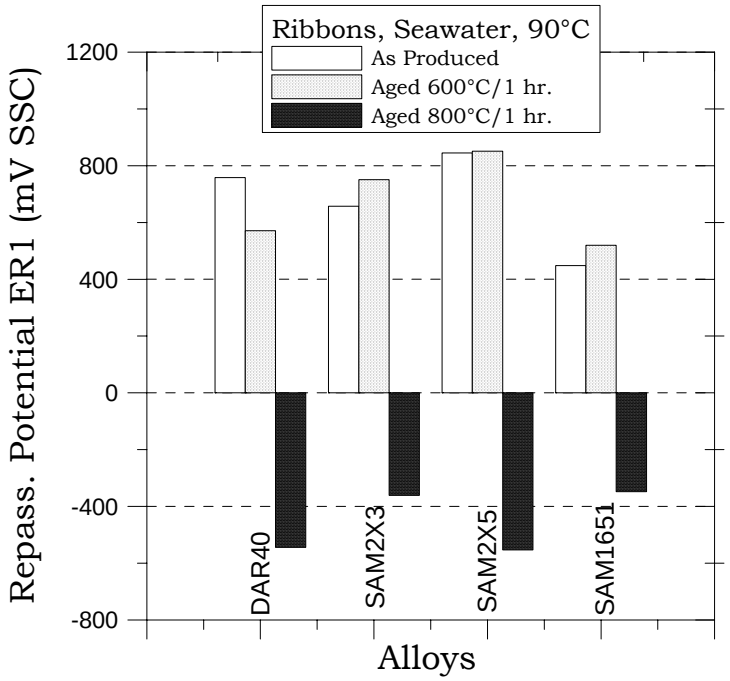

Figure 9. Repassivation potential ER1 for the four ribbon materials tested. Effect of thermal treatment

Summary and Conclusions

- Iron-based amorphous metals (ribbons) have an extraordinary resistance to localized corrosion by chloride, far superior than Ni-Cr-Mo alloys.
- When the amorphous ribbons are heated at 800°C for 1 hr they lose their localized corrosion resistance. This loss in corrosion resistance is attributed to a devitrification (or re-crystallization) process

Acknowledgements

This work was performed under the auspices of the U. S. Department of Energy by the University of California Lawrence Livermore National Laboratory under contract W-7405-Eng-48. Work was sponsored by the United States Department of Energy (DOE), Office of Civilian Radioactive Waste Management (OCRWM) and the Defense Advanced Research Projects Agency (DARPA), Defense Science Office (DSO). The guidance of Leo Christodoulou at DARPA DSO and of Jeffrey Walker at DOE OCRWM is gratefully acknowledged.

Disclaimer

their employees, makes any warranty, express or implied, or assumes any legal liability or responsibility for the accuracy, completeness, or usefulness of any information, apparatus, product, or process disclosed, or represents that its use would not infringe privately owned rights. Reference herein to any specific commercial product, process, or service by trade name, trademark, manufacturer, or otherwise, does not necessarily constitute or imply its endorsement, recommendation, or favoring by the United States Government or the University of California. The views and opinions of authors expressed herein do not necessarily state or reflect those of the United States Government or the University of California, and shall not be used for advertising or product endorsement purposes.

References

1. J. R. Scully and A. Lucente, "Corrosion of Amorphous Metals," ASM Handbook, Volume 13B, Corrosion: Materials, p. 476 (ASM International, 2005: Materials Park, OH).
2. K. Hashimoto, K. Asami, M. Naka and T. Masumoto, Corr. Sci., 19, 857 (1979)
3. K. Asami, M. Naka, K. Hashimoto and T. Masumoto, J. Electrochem. Soc., 127, 76 (1991).
4. H. Habazaki, A. Kawashima, K. Asami and K. Hashimoto, J. Electrochem. Soc., 138, 2130 (1980).
5. R. B. Rebak, L. F. Aprigliano, S. D. Day, and J. C. Farmer, "Salt Fog Testing of Iron-Based Amorphous Alloys," Paper NN3.14, in proceedings of the symposium Scientific Basis for Nuclear Waste Management XXX in the Materials Research Society annual conference, 28 November to 01 December 2006, Boston MA.
6. J. R. Scully, A. Gebert and J. H. Payer, submitted for publication, 2006
7. R. B. Rebak and J. H. Payer, "Passive Corrosion Behavior of Alloy 22," in proceedings of the International High-Level Radioactive Waste Management –IHLRWM-Conference, p. 493, Las Vegas, NV April 30 to May 04, 2006, (American Nuclear Society, La Grange Park, IL).
8. J. C. Farmer, J. J. Haslam, S. D. Day, D. J. Branagan, C. A. Blue, J. D. K. Rivard, L. F. Aprigliano, N. Yang, J. H. Perepezko and M. B. Beardsley, "Corrosion Characterization of Iron-Based High-Performance Amorphous-Metal Thermal-Spray Coatings," in proceedings of 2005 ASME PVP Conference 17-21 July 2005, Vol. 7, Operations, Applications and Components, p. 583 (New York, NY: ASME, 2005).
9. J. Shen, Q. Chen, J. Sun, H. Fan and G. Wang, Applied Physics Letters, 86, 151907 (2005).
10. L. Kaufman, J. H. Perepezko, and K. Hildal "Synthesis and Performance of Fe-Based Amorphous Alloys for Nuclear Waste Repository Applications," in proceedings of the Joint International Topical Meeting on Mathematics and Computation and Supercomputing in Nuclear Applications (M&C + SNA), organized by the American Nuclear Society in Monterey, CA 15-19 April 2007.

11. T. Lian, S. D. Day, P. D. Hailey, J. S. Choi and J. C. Farmer, "Comparative Study on the Corrosion Resistance of Fe-Based Amorphous Metal, Borated Stainless Steel and Ni-Cr—Mo-Gd Alloy," Paper NN8.7 in proceedings of the symposium Scientific Basis for Nuclear Waste Management XXX in the Materials Research Society annual conference, 28 November to 01 December 2006, Boston MA.

12. J. C. Farmer "Corrosion-Resistant Iron-Based Amorphous-Metal Coatings," Paper PVP2006-ICPVT11-93421 in the 2006 Pressure Vessels & Piping Conference and the Eleventh International Conference on Pressure Vessel Technology, 23-27 July 2006, Vancouver, BC, Canada.

13. R. B. Rebak, S. D. Day, T. Lian, L. F. Aprigliano, P. D. Hailey and J. C. Farmer, "Enhanced Corrosion Resistance of Iron-Based Amorphous Alloys," Paper PVP2007-26166 in Proceedings of PVP2007 2007 ASME Pressure Vessels and Piping Division Conference, July 22-26, 2007, San Antonio, Texas.

14. ASTM International, Volume 03.02, Corrosion of Metals, (ASTM International, 2004: West Conshohocken, PA).